ACS OMEGA

Article

http://pubs.acs.org/journal/acsodf

# Discrepancies between Cyclic and Linear Antimicrobial Peptide Actions on the Spectrochemical and Nanomechanical Fingerprints of a Young Biofilm

Oona Freudenthal,[†,‡] Fabienne Quilès,*[,†,‡] and Grégory Francius*[,†,‡]

[†]Université de Lorraine, Laboratoire de Chimie Physique et Microbiologie pour l'Environnement, LCPME, UMR 7564, Villers-lès-Nancy, F-54600, France

[‡]CNRS, Laboratoire de Chimie Physique et Microbiologie pour l'Environnement, LCPME, UMR 7564, Villers-lès-Nancy, F-54600, France

**ABSTRACT:** Antimicrobial peptides (AMPs) are currently known for their potential as an alternative to conventional antibiotics and new weapons against drug-resistant bacteria and biofilms. In the present work, the mechanism of action of a cyclic (colistin) and a linear (catestatin) AMP on a young *E. coli* biofilm was deciphered from the molecular to the cellular scale. To this end, infrared spectroscopy (attenuated total reflection−Fourier transform infrared) assisted by chemometric analysis was combined with fluorescence and atomic force microscopies to address the very different behaviors of both AMPs. Indeed, the colistin dramatically damaged the bacterial cell wall and the metabolism even though its action was not homogeneous over the whole bacterial population and repopulation can be observed after peptide removal. Conversely, catestatin did not lead to major damages in the bacterial morphology but its action was homogeneous over the whole bacterial population and the cells were unable to regrow after the peptide treatment. Our results strongly suggested that contrary to the cyclic molecule, the linear one is able to cause irreversible damages in the bacterial membrane concomitantly to a strong impact on the bacterial metabolism.

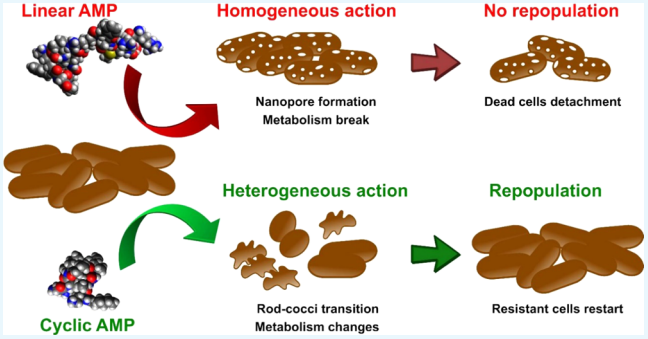


## 1. INTRODUCTION

In the past decades, overconsumption of antibiotics associated with fast bacterial growth and strong facility to adapt to external constraints has resulted in an important emergence of multidrug-resistant bacteria. Among the multidrug-resistant microorganisms, the case of pathogenic bacteria is a global emergency and the design of new antimicrobial treatments and molecules with chemical characteristics different from those of current antibiotics represents an urgent issue.[1−4] Besides, the treatment of bacterial infections has become very challenging, notably when pathogenic bacteria are organized in a biofilm. The biofilm is a three-dimensional assembly of microorganisms embedded in a self-produced exopolymeric matrix attached on biological or abiotic surfaces.[5] Several studies highlighted that conventional antibiotic's effectiveness against planktonic bacteria can be totally inefficient against sessile cells mainly because microbial biofilms are intrinsically much more resistant to antibiotics.[6−8] The reduced biocide susceptibility of bacteria in biofilms can originate from delayed penetration of the antimicrobial, an alteration of the cellular growth rate in the biofilm, from adaptive responses (repression or induction of genes), and the occurrence of persisters even in young biofilms. The design of alternative strategies to conventional antibiotics is of major importance particularly for a more efficient anti-biofilm treatment.

In this context, antimicrobial peptides (AMPs) are considered as an alternative to conventional antibiotics and potentially a more efficient weapon against bacteria and biofilms mainly because they are less susceptible to give rise to bacterial drug-resistance due to their nonspecific action toward bacteria.[9−12] AMPs are short biomolecules exhibiting various structures and physicochemical properties. AMPs are generally composed of less than 100 amino acid residues, and their primary structure can be either linear or cyclic.[13] AMPs can be classified in four families according to their secondary structures, including $\alpha$-helices, $\beta$-sheets, mixed structures, and linear or extended secondary structure.[9,14] AMPs are often amphipathic (i.e., containing both hydrophobic and hydrophilic domains) and are often positively charged.[9,14,15] Most AMPs act first by electrostatic interactions with the negatively charged bacterial cell wall.[16] After this first step, accumulation and conformational changes that occur at the bacterial interface are followed generally by the membrane disruption. Besides, the activity of AMPs can also disturb and interfere in metabolic and intracellular processes, leading to inhibition of cell wall, nucleic acid, or protein biosynthesis.[17,18] Usually, linear and short

**Received:** May 22, 2017
**Accepted:** August 30, 2017
**Published:** September 18, 2017

  

DOI: 10.1021/acsomega.7b00644
*ACS Omega* 2017, 2, 5861−5872

**Table 1. Primary Structure and Peptide Properties of Colistin and Catestatin**

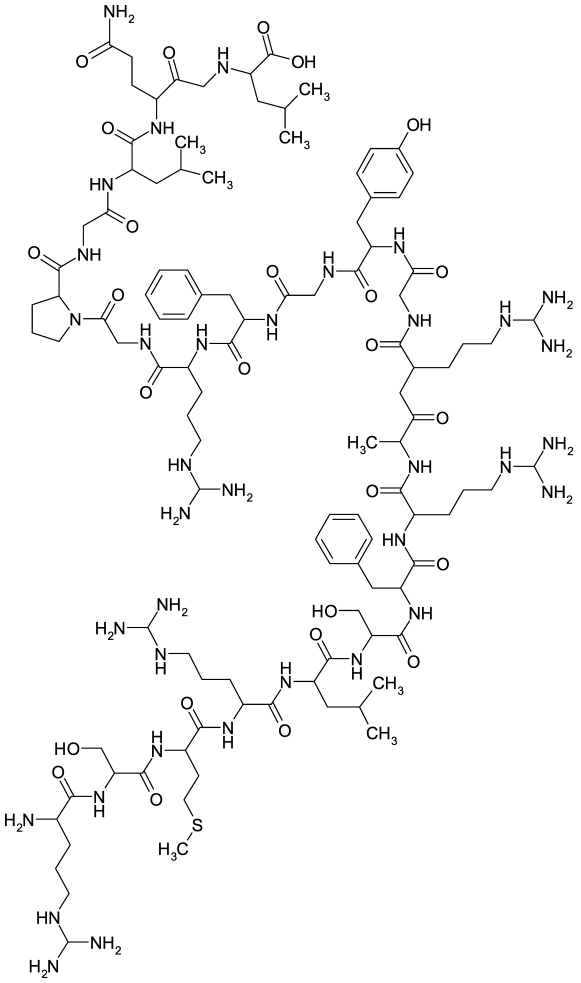

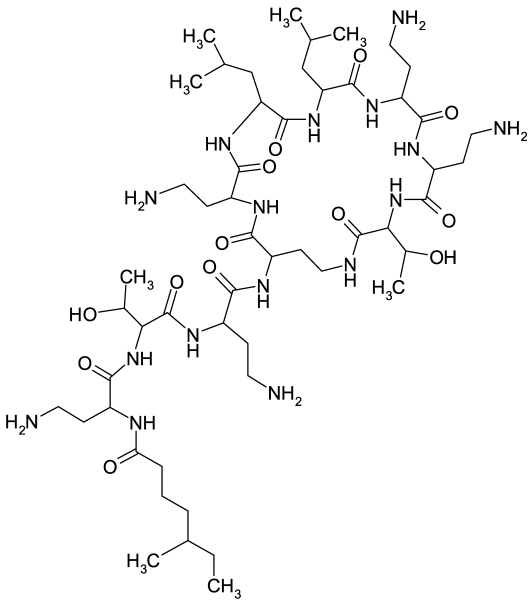

| peptide properties | catestatin | colistin |
|---|---|---|
| primary structure | linear | cyclic |
| length (a.a.) | 21 | 10 |
| mass (g/mol) | 2424.30 | 1155.43 |
| isoelectric point (pI) | 12.7 | 8.3 |
| net charge | +5 | +5 |
| hydrophobic amino acids | 8 | 8 |
| acyl chain | no | yes |

AMPs are nonstructured in water and they adopt a secondary structure only upon interaction with the membrane.[19] Converse to linear AMPs, some cyclic AMPs are able to adopt a specific structure even in water.[20] Moreover, previous studies evidenced that the cyclic molecules are amongst the most effective antimicrobial agents.[13,21] If the AMPs also include either nonnatural amino acids or alkyl chains in their primary structure, they gain a broader antibacterial activity.[22,23]

Catestatin is a linear peptide composed of 21 amino acids and exhibits antimicrobial activity against a wide array of pathogens.[24] This peptide is a fragment of chromogranin A and is well known for stimulating the immune system cells and for its nontoxicity to mammalian cells.[25,26] Catestatin has been shown to have strong antimicrobial activity also in multifunctional coatings on titanium implants.[27] Colistin, a cyclic decapeptide linked to a fatty acid chain, belonging to the polymyxin family, is known for its antimicrobial action against multidrug-resistant bacteria.[28,29] Colistin is highly efficient on Gram-negative bacteria, but its use is hampered by its nephro- and neurotoxicity (Table 1).[30]

In the present work, we compare the antimicrobial activity of cyclic colistin and linear catestatin on a young *E. coli* biofilm to investigate the influence of the structure on their activity and mechanism of action. Attenuated total reflectance Fourier transform infrared spectroscopy (ATR-FTIR) assisted by Bayesian positive source separation (BPSS) chemometric analysis, atomic force microscopy (AFM), and epifluorescence microscopy were combined to monitor in situ and in real time the action of both peptides. ATR-FTIR allows the investigation of metabolic and biochemical changes within the biofilm, whereas AFM was used to visualize the local effects of the antimicrobial peptide upon cell morphology and mechanical properties. In addition, the bacterial membrane integrity was tested by staining of the biofilms with the *Bac*Light kit.



DOI: 10.1021/acsomega.7b00644
*ACS Omega* 2017, 2, 5861−5872

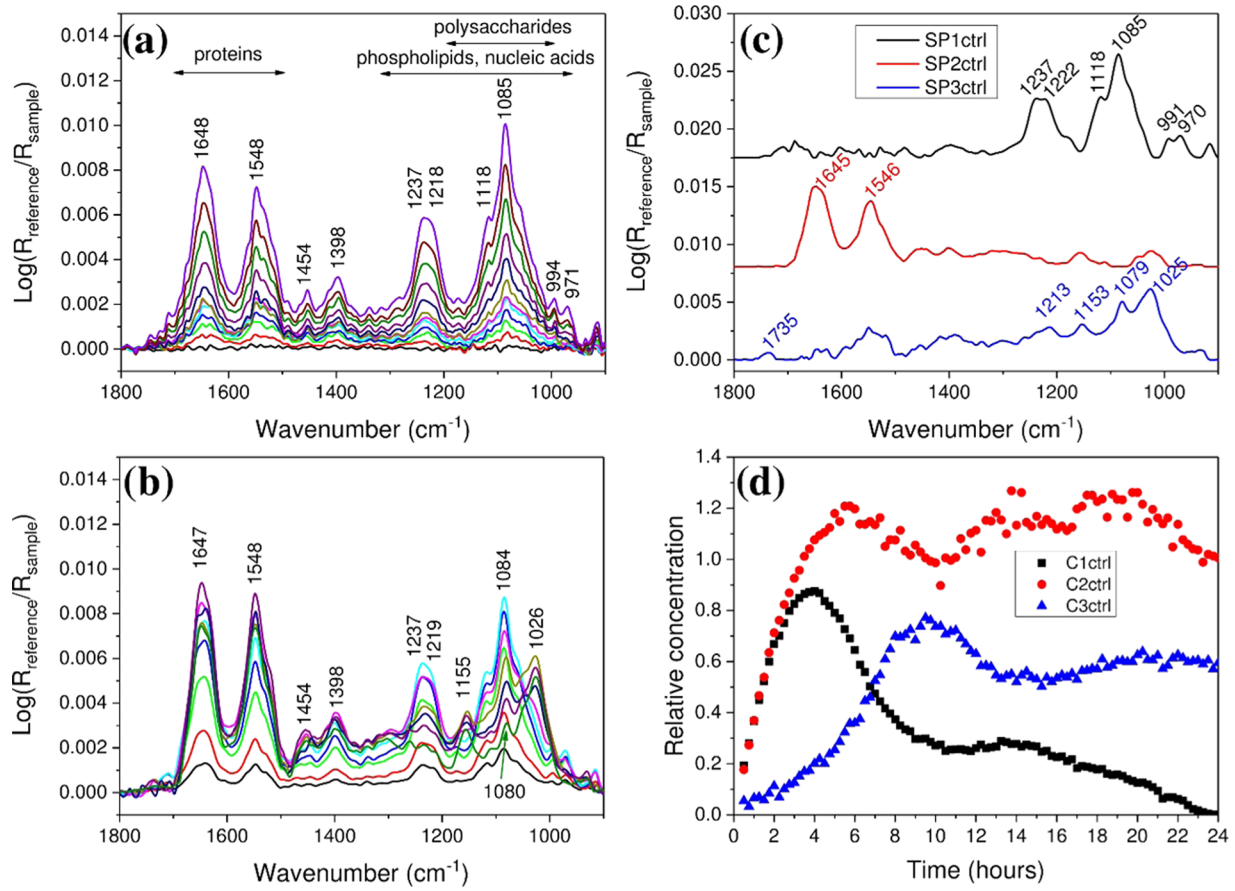


**Figure 1.** Time evolution of the ATR-FTIR spectra during the growth of the *E. coli* biofilm (a) during the first 5.5 h (spectra at 0, 0.5, 1, 1.5, 2, 2.5, 3, 3.5, 4, 5, and 5.5 h); (b) during the flow of LB/10 for 24 h in closed circulation, the reference is the spectrum of the 5.5 h old *E. coli* biofilm (spectra at 1, 2, 3, 4, 5, 6, 10, 14, 20, and 24 h of flow); (c) estimated BPSS ATR-FTIR pure component spectra; and (d) corresponding concentration profiles extracted from the 95 spectra recorded during the flow of sterile LB/10. Offsets of spectra are used for clarity.

**Table 2. Assignments of Principal Infrared Vibrational Bands of the Fingerprint Region (1800−900 $cm^{-1}$) of the ATR-FTIR Spectrum of *E. coli* Biofilm on Germanium Crystal**[a]

| wavenumber ($cm^{-1}$) | vibration | attribution |
|---|---|---|
| 1730−1740 | $\nu$ > C═O | lipid ester |
| ~1645 | amide I ($\nu$C═O, $\nu$C−N, $\delta$N−H) | proteins |
| ~1550 | amide II ($\delta$N−H, $\nu$C−N) | proteins |
| ~1455 | $\delta CH_n$ ($n$ = 2, 3) | lipids |
| 1398 | $\nu_s COO^-$ | proteins, lipids |
| ~1300 | amide III ($\nu$C−N, $\delta$N−H) | proteins |
| 1236−1221 | $\nu_a PO_2^-$ | phosphodiesters, nucleic acids, phospholipids, lipopolysaccharides |
| 1154 | $\nu_s$C−OH, $\nu$C−O | polysaccharides, proteins |
| 1086 | $\nu_s PO_2^-$ | phosphodiesters, phospholipids, nucleic acids, lipopolysaccharides |
| 1160−950 | $\nu_s$C−O−C, $\nu_s$P−O−C (R−O−P−O−R′) | polysaccharides |

[a]Key: *a*, antisymmetric; *s*, symmetric; $\nu$, stretching; $\delta$, bending.

## 2. RESULTS AND DISCUSSION

### 2.1. *E. coli* Biofilm before the Peptide Treatment.

Figure 1a illustrates the evolution of the ATR-FTIR spectra during the initial steps of biofilm formation in the fingerprint region. The infrared band assignments were made according to the literature[31−35] and are gathered in Table 2. The amide I and II bands from proteins are located at 1648 and 1548 $cm^{-1}$, respectively. The region 1340−1190 $cm^{-1}$ is assigned to the antisymmetric stretching of the phosphate groups of nucleic acids and phospholipids as well as the amide III band of proteins. Finally, a large massif is observed in the region 1160−950 $cm^{-1}$, which is attributed to the vibrational modes of polysaccharides as well as to the symmetric stretching of the phosphate groups of phospholipids and nucleic acids. The intensities of the whole bacterial ATR-FTIR fingerprint increased, reflecting the attachment and colonization of bacteria onto the Ge crystal. Furthermore, the intensities of the bands associated to nucleic acids and polysaccharides (between 1160 and 950 $cm^{-1}$) increased at a higher rate than those of the amide II band (at 1547 $cm^{-1}$) during the flow of sterile LB/10 from 2.5 to 5.5 h and corresponded to a high metabolic activity for bacterial cell division and biofilm growth. The 5.5 h old



DOI: 10.1021/acsomega.7b00644
ACS Omega 2017, 2, 5861−5872

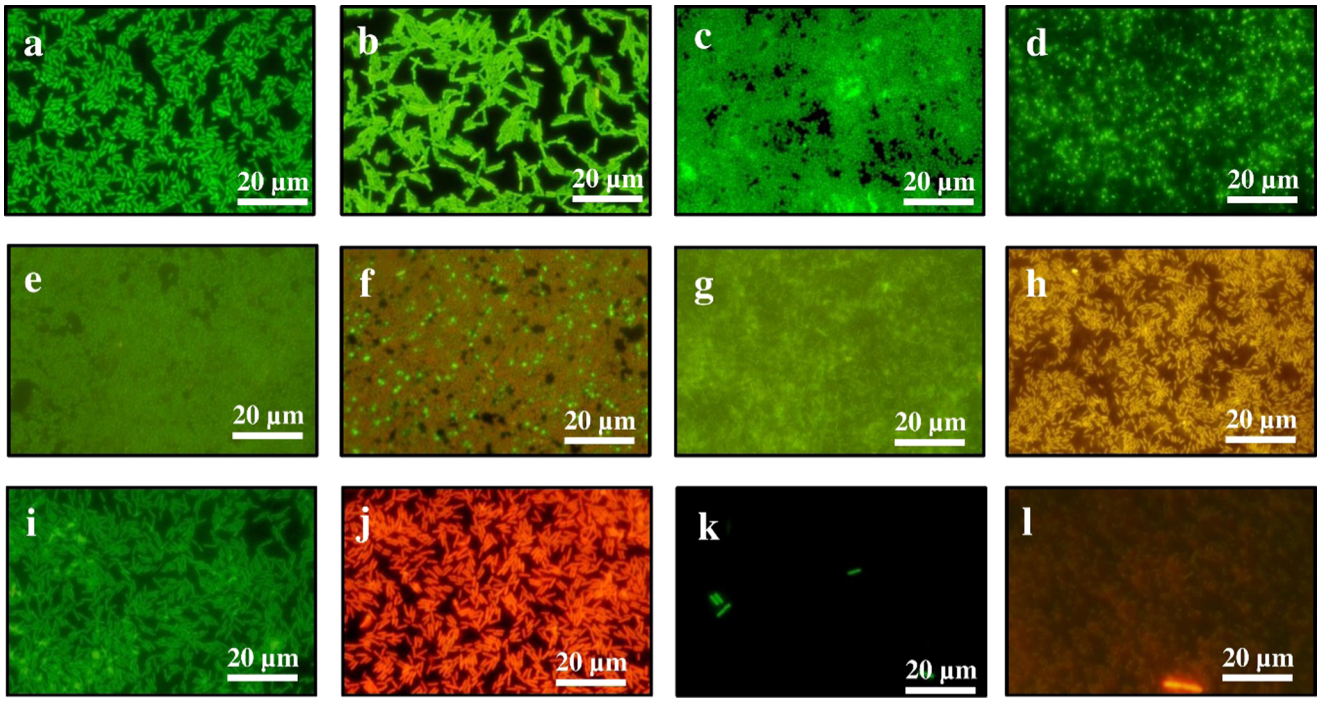


**Figure 2.** Representative epifluorescence images of nonstained (a, e, i, c, g, and k) and *Bac*Light stained (b, f, j, d, h, and l) *E. coli.* (a, b) 5.5 h old biofilm; (c, d) 29.5 h old biofilm after the flow of LB/10 without antimicrobial peptide (control); (e, f) 24 h colistin (0.87 $\mu$M) treated; (i, j) 24 h catestatin (60 $\mu$M) treated; (g, h) 24 h colistin (0.87 $\mu$M) treated after additional 17 h LB/10 circulation; and (k, l) 24 h catestatin (60 $\mu$M) treated after additional 17 h LB/10 circulation. Exposure times: (a–d) 100, (e) 7000, (f) 280, (g) 500, (h) 570, (i) 3000, (j) 240, (k–l) 250 ms.

biofilm was mostly composed of a bacterial monolayer, including some bacterial clusters, as observed by epifluorescence microscopy (Figure 2a,b), with an average surface coverage of 40 ± 11%. The bacteria stained with the *Bac*Light kit were green (Figure 2b), suggesting that their membranes were intact. The bacteria had an average length of 2.9 ± 0.9 $\mu$m and a diameter of 0.9 ± 0.1 $\mu$m (calculated from at least 10 randomly selected individual bacteria).

A closer look on the bacterial morphology on the nanoscale was carried out by AFM imaging (Figure 3). This small region of 5 × 5 $\mu m^2$ surface area was almost totally covered by rod-shaped bacteria. Cells exhibited an average length of about 2.3 ± 0.6 $\mu$m for a width of 0.8 ± 0.1 $\mu$m (Table 3), in accordance with epifluorescence images. The height profiles (Figure 3c) showed depth variations of about 300–700 nm, corresponding to the bacterial height after slight dehydration. The estimated average height of the bacterial cells was thus 303 ± 44 nm (see Table 3). Such values are generally measured when bacteria lose partly their intracellular cytosol.[36]

**2.2. *E. coli* Biofilm Development without Peptide Treatment (Control Experiment).** The 5.5 h old biofilm was exposed for 24 h to sterile LB/10 medium in a closed circuit. Figure 1b shows the ATR-FTIR spectra recorded during 24 h closed circulation of LB/10 medium. During the first 2.5 h of LB/10 flow, characteristic spectra of bacteria were recorded.[31] The intensities of these infrared bands increased, suggesting bacterial growth on the crystal. After this period, the amide band intensities remained stable without significant changes in the band shape. After 6 h of LB/10 flow, bands assigned to nucleic acids at 1237, 1219, and 1086 $cm^{-1}$ started to decrease and bands at 1155, 1080, and 1026 $cm^{-1}$ started to increase. The latter bands were assigned to glycogen.[37] Glycogen is a storage compound, and it is generally biosynthesized when nutritive compounds such as nitrogen and/or phosphorus are lacking and carbon is in excess.[38] As the LB/10 circulation was closed, no continuous flow of fresh nutrients was available for the bacteria, leading to impoverishment of the growth medium in some nutrients. The BPSS procedure of curve resolution was used to help the interpretation of the spectra that had overlapped regions and smooth continuous spectral evolutions.[37] Three pure component spectra, which explained 96% of the total spectral variation of the spectra set, were extracted. The percentage of nonreconstructed data was mainly noise, and represented only 4% of the total spectral variation of the spectra set. The extracted pure spectra reflect the main components to be varying with a significant statistical variance during the biofilm development and give a time-dependent image of the physiological changes occurring in the sessile bacteria. Spectra of pure components SP1ctrl, SP2ctrl, and SP3ctrl (Figure 1c) have the general spectral features of nucleic acids, proteins, and glycogen, with probably phospholipids (bands at 1735 and 1213 $cm^{-1}$), respectively.[39,40] The assignment of these pure component spectra allowed tracing the concentrations of the corresponding biomolecules during the biofilm development. Figure 1d shows the relative concentration profiles calculated by the BPSS analysis. The estimated relative concentrations of each pure component spectrum showed different time evolutions. The relative concentration C1ctrl and C2ctrl of pure components PS1ctrl and PS2ctrl, respectively, increased together during the first 4 h of LB/10 flow. The sum of both spectra represented very well the spectral feature of bacteria and suggested the growth of bacteria on the crystal surface. The quite stable quantity of protein after 6 h of the LB/10 flow suggested a quite stable bacterial population in direct contact with the crystal. Some spatial reorganization between 10 and 12 h and after 24 h of LB/10 flow can be suggested from the small fluctuations of C2ctrl (Figure 1d). The nucleic acid component decreased after 4 h of LB/10 flow (SP1ctrl and C1ctrl, Figure



DOI: 10.1021/acsomega.7b00644
*ACS Omega* 2017, 2, 5861–5872

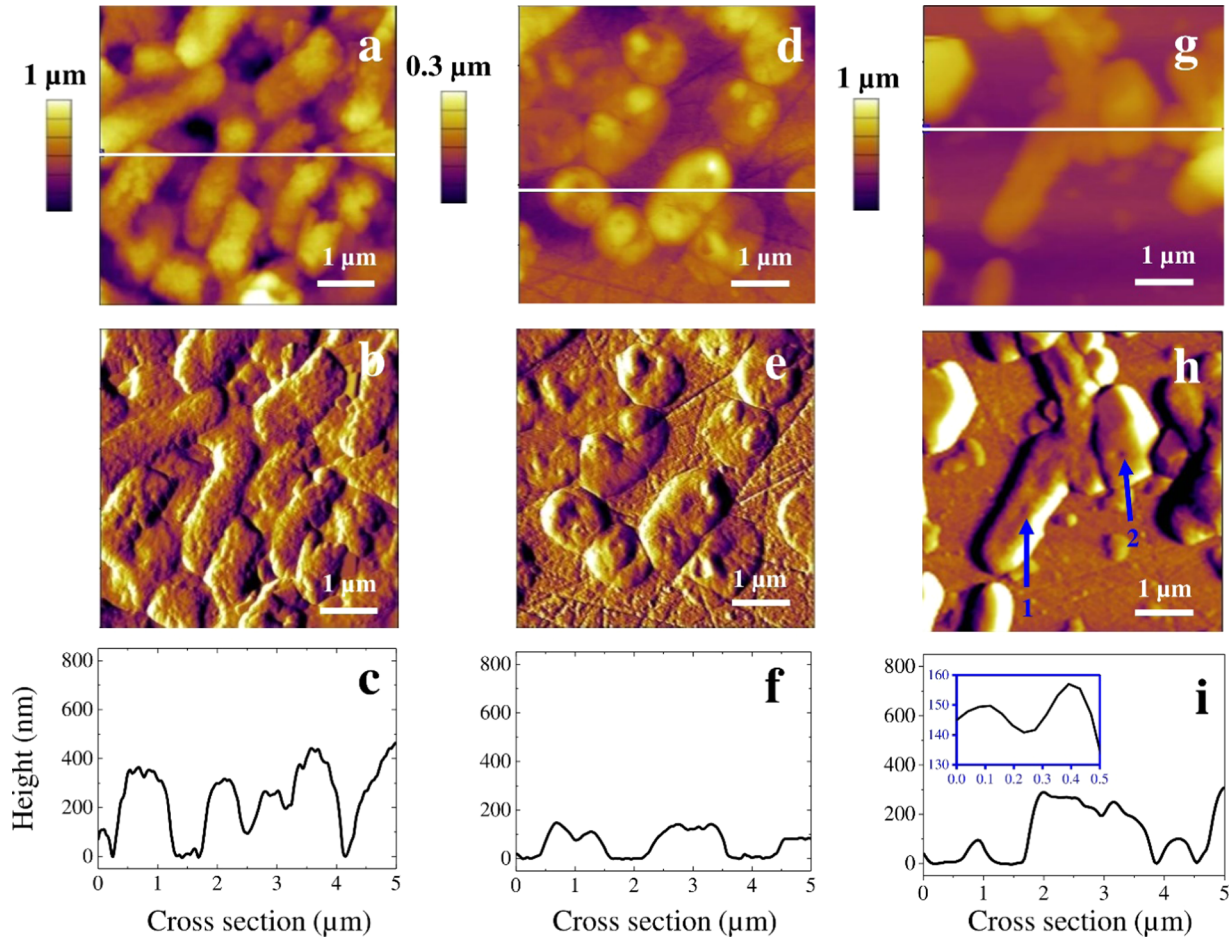


**Figure 3.** AFM images (lateral size 5 $\mu$m) showing the morphology of a (a–c) 5.5 h old *E. coli* reference; (d–f) 24 h colistin (0.87 $\mu$M) treated; and (g–i) 24 h catestatin (60 $\mu$M) treated biofilm. Height images: a, d, and g; deflection images: b, e, and h; height profiles: c, f, and i (height profiles corresponding to the lateral cross sections indicated by the white lines). The blue inset in (i) corresponds to the cross section of the hole #1 indicated in (h) by the blue arrow.

**Table 3. Morphological and Mechanical Properties of Bacteria Constituting the Biofilm Measured by AFM**

| treatments | height (nm)[a] | length ($\mu$m)[a] | width (nm)[a] | Young modulus (kPa)[b] |
|---|---|---|---|---|
| prior to treatment | 303 ± 44 | 2.29 ± 0.64 | 0.78 ± 0.07 | 135 ± 89 |
| colistin | 76 ± 18 | 1.63 ±0.17 | 1.10 ± 0.10 | 598 ± 277 |
| catestatin | 382 ± 44 | 2.15 ± 0.33 | 0.83 ± 0.09 | 48 ± 27 |

[a]Values calculated on the average of 10 randomly taken individual bacteria. [b]Young's modulus calculated from an average of three force–volume images (excluding force curves recorded on the germanium substrate) containing at least 5–10 bacteria. Force measurements (1024 force curves for each FVI) were performed in phosphate-buffered saline (PBS) medium at room temperature.

1d) and finally was canceled after 24 h (i.e., it fell at about the same level as the one for the 5.5 h old biofilm). This showed that the bacteria at the bottom of the biofilm gradually decreased their metabolic activity as a function of time. The biosynthesis of glycogen began as soon as 3 h of the LB/10 flow. The quantity of synthetized glycogen increased continuously over 10 h (SP3ctrl and C3ctrl, Figure 1c,d) and then slightly decreased until reaching a plateau value between 13 and 24 h of LB/10 flow. After 13 h, the quantity of the glycogen stayed constant and it was concomitant to the end of nucleic acid synthesis. The end of the synthesis and degradation of the ARN were probably associated with the ageing of the bacteria that grew slowly or that stopped growing and stopped the biosynthesis of glycogen within about 1 $\mu$m over the Ge crystal, as this feature was already observed in sessile bacteria of *P. fluorescens*.[37] Figure 2c,d illustrates the epifluorescence images of the control biofilm. The bacteria were mainly arranged in a monolayer on the surface with multilayered bacteria at some places, and the average coverage was estimated to be 71 ± 19%. The bacteria stained with the *Bac*Light kit were green, indicating intact cell membranes. The average length of bacteria in the 29.5 h old biofilm was significantly smaller than that of bacteria in the 5.5 h old biofilm. It was estimated to be 1.8 ± 0.4 $\mu$m, whereas the width only slightly changed (Table 4), suggesting that the bacteria probably adapted their growth to the current microenvironment.[41]

**2.3. *E. coli* Biofilm Treated with Colistin.** The minimal inhibitory concentration (MIC) of colistin for planktonic *E. coli* was estimated at 0.87 $\mu$M. This concentration is below the concentration at which colistin form aggregates.[42] Figure 4a shows the ATR-FTIR spectral evolution during 24 h of colistin exposure at 0.87 $\mu$M. An increase of the amide I and II bands intensities at 1647 and 1547 $cm^{-1}$, respectively, during the first 9 h was observed. The spectra also showed a slight increase of the bands assigned to nucleic acids at 1240, 1222, 1118, and 1064 $cm^{-1}$ during the first 2 h of colistin circulation. Then, they



DOI: 10.1021/acsomega.7b00644
*ACS Omega* 2017, 2, 5861–5872

**Table 4. Morphological Characteristics of Bacteria Constituting the Biofilm, Determined by Optical Epifluorescence Microscopy**[a]

| treatments | length ($\mu$m) | width ($\mu$m) |
|---|---|---|
| none (5.5 h reference biofilm) | 2.95 ± 0.87 | 0.88 ± 0.13 |
| none (control) | 1.77 ± 0.41 | 0.74 ± 0.12 |
| colistin | 1.55 ± 0.16 | 0.70 ± 0.09 |
| catestatin | 3.07 ± 0.53 | 0.76 ± 0.12 |

[a]Values were calculated on the average of 30 randomly taken individual bacteria from the GFP (entry) side of the crystal.

decreased after 4 h of circulation, reflecting a decrease in nucleic acid production and thus the drop in metabolic activity,[36] also illustrated by a very weak production of glycogen (Figure 4a, weak bands at 1055 and 1024 $cm^{-1}$). The BPSS procedure resolved three pure component spectra (Figure 5a), which explained 97% of the total spectral variation of the spectra set. SP1col had the general spectral features of nucleic acids, SP2col had the general spectral features of nucleic acids (negative bands) and of glycogen (positive bands), and SP3col had the spectral features of proteins.[39,40] Figure 5b shows the relative concentration profiles calculated by the BPSS analysis. The estimated relative concentrations C1col and C2col of SP1col and SP2col, respectively, showed the decrease of the nucleic acid biosynthesis, as soon as 2 h of colistin treatment. However, a weak biosynthesis of glycogen was maintained. The colistin treatment of the young biofilm changed drastically the bacterial metabolism, but some of the processes observed in the control biofilm were poorly maintained. C3col of SP3col, which represented the protein variation in the young biofilm, increased during 8 h and then slightly decreased non-monotonously. This feature was mainly assigned to the increase of the number of bacteria on the surface. The possible accumulation of colistin cannot be clearly evidenced because its initial concentration was too low. This conclusion was supported by the epifluorescence images recorded after 24 h of colistin treatment. Representative fluorescence images of biofilms after incubation with colistin are presented in Figure 2e,f. The bacteria within the 29.5 h old biofilm exhibited a very weak self-fluorescence presumably due to a very low GFP production. Because of the poor contrast of the images, it was not possible to calculate an accurate average ratio of the coverage. However, this coverage ratio was qualitatively higher than that for the 5.5 h old biofilm. These results were in accordance with the infrared spectra that suggested a weaker bacterial metabolic activity that however did not cancel the growth of bacteria on the Ge crystal. The images of the biofilm stained with the *Bac*Light kit showed a heterogeneous population of bacteria composed of a large amount of damaged bacteria (orange/red), some bacteria with nondamaged

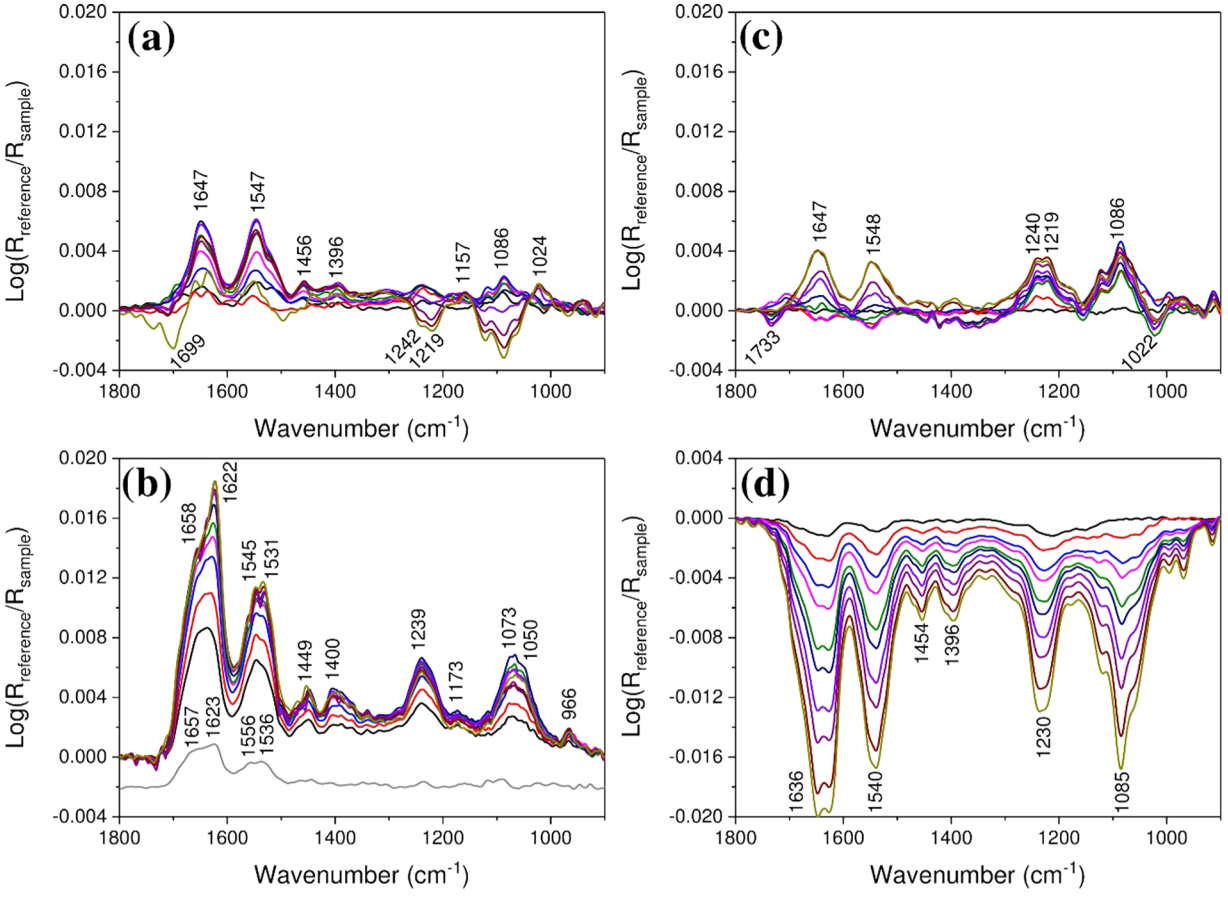


**Figure 4.** Time evolution of the ATR-FTIR spectra of the *E. coli* biofilm during (a) 24 h colistin (0.87 $\mu$M) treatment; (b) 24 h catestatin (60 $\mu$M) treatment, the gray spectrum at the bottom is the spectrum of catestatin at 60 $\mu$M after 12 h of flow in abiotic conditions; (c) 17 h open circulation of LB/10 postcolistin treatment; (d) 17 h open circulation of LB/10 postcatestatin treatment. The reference spectra are the spectra of the 5.5 h old biofilm of *E. coli* for (a) and (b) and the spectrum after the flow of the antimicrobial peptide during 24 h for (c) and (d). (spectra at 1, 2, 3, 4, 5, 6, 10, 14, 20, and 24 h of the peptide flow for a, b and at 0.25, 1, 2, 3, 5, 6, 8, 10, 14, and 17 h of LB/10 flow for c, d).



DOI: 10.1021/acsomega.7b00644
*ACS Omega* 2017, 2, 5861−5872

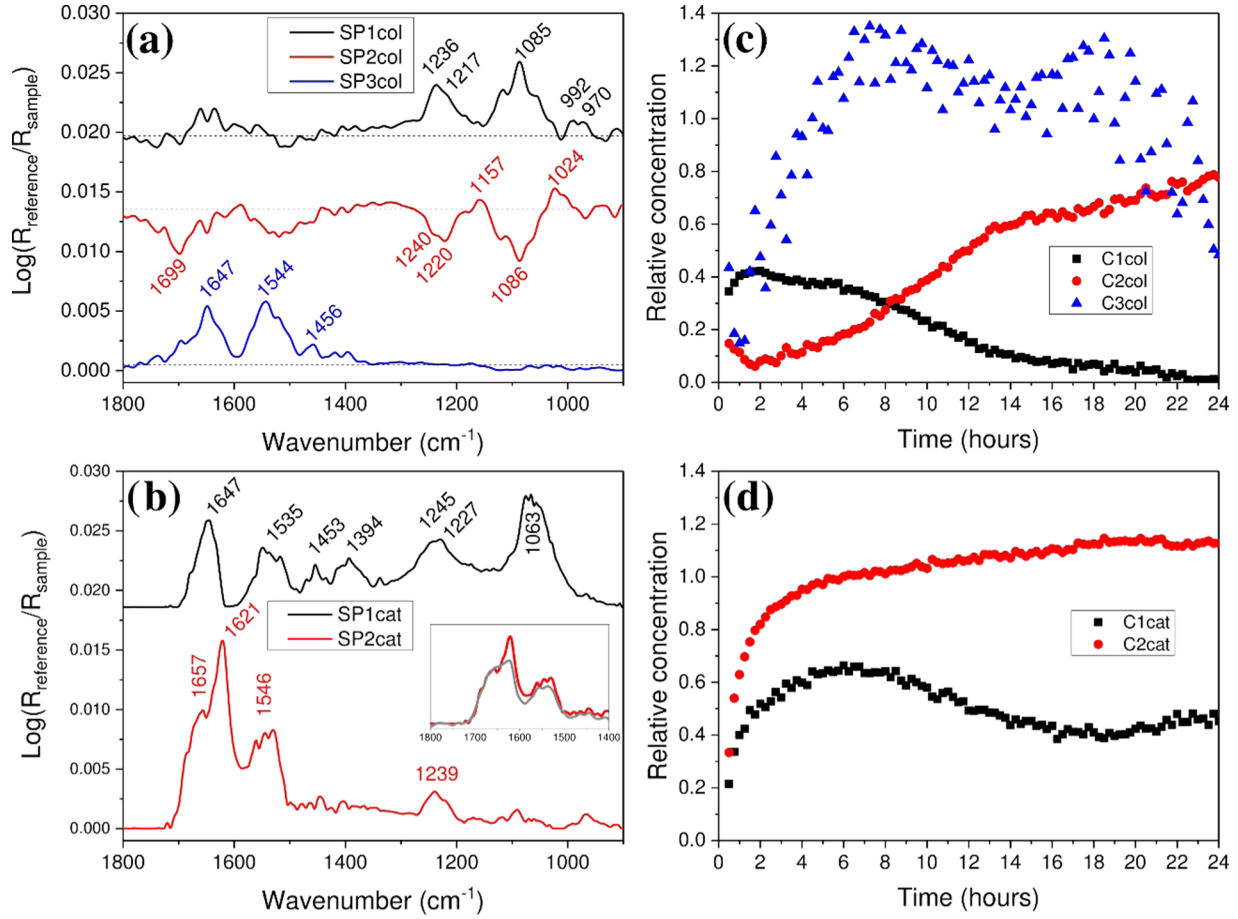


**Figure 5.** Estimated BPSS ATR-FTIR pure component spectra (a, b) and corresponding concentration profiles (c, d): (a, c) experiment with 24 h of colistin treatment; (b, d) experiment with 24 h of catestatin treatment. Offsets of spectra are used for clarity. Inset in (b): comparison of the experimental spectrum of catestatin in solution and the calculated spectrum SP2cat.

membranes (green), and cell fragments (dark green blurred background in Figure 2f). In addition, dramatic changes in the morphology with coccoid-shaped and smaller bacteria of ∼1.6 $\mu$m length with ∼0.7 $\mu$m diameter were observed (Table 4). This result was in accordance with the findings of Soon et al. who reported colistin-susceptible *Acinetobacter baumannii* to adopt a rod-shaped morphology.[43] The occurrence of bacteria with nondamaged membranes suggested that either the colistin concentration was not sufficient to reach all of the bacteria in the biofilm or the cells might have expressed a resistance/persistence already described.[44,45]

Figure 3d,e illustrates the AFM images (height and deflection) and cross section (Figure 3f) obtained from the 5.5 h old biofilm subjected to colistin at 0.87 $\mu$M for 24 h. They are very different from those recorded on the 5.5 h old biofilm before the peptide treatment. The bacterial shape transition was also observed with the occurrence of coccoid or spherical cells of about 1.6 ± 0.2 $\mu$m (Table 3). These data confirmed that bacterial cell walls were strongly damaged in the presence of colistin. The cross sections (Figure 3f) showed a dramatic decrease of the bacterial thickness, with values of about 50−150 nm instead of 350−450 nm before the treatment (Table 3). This result underlined that the antimicrobial peptide should modify the bacterial membrane permeability and consequently must have an impact on the mechanical properties of the bacterial cell wall. Figure 6 shows typical force−indentation curves and elasticity histograms recorded on the biofilm before and after the colistin treatment. As evidenced in Figure 6a, the maximal indention depth measured at an applied force of 4 nN on the representative force curves was about 280 and 130 nm for the nontreated and colistin-treated biofilm, respectively. These elements indicated clearly an increase of the bacterial stiffness when the latter was exposed to colistin. Such results are in line with the *Bac*Light assays and the differences in bacterial morphology observed after the colistin treatment. The analysis of the whole force curves recorded before and after the action of the AMPs with the Sneddon model allowed us to calculate the stiffness statistic distribution (Figure 6b). The nontreated biofilm yielded a pseudo Gaussian behavior of the elastic modulus distribution, with an average value of 135 ± 89 kPa. This value is in the same range as the one that has been measured in the planktonic form in previous works.[46] When the biofilm was treated with colistin, the Gaussian behavior of the elastic modulus distribution was lost and the latter became very wide, with an average value of 598 ± 277 kPa. An increase of cell rigidity has already been described upon the colistin action on several bacterial strains.[47−49] These works highlighted that colistin dramatically impacted both bacterial turgor pressure and cell wall stiffness even though the concentration was lower than that of bacterial MIC. The authors explained such stiffening in bacterial rigidity by both colistin accumulation at the outer membrane until saturation of specific LPS binding sites and colistin association with the peptidoglycan layer.[49]



DOI: 10.1021/acsomega.7b00644
*ACS Omega* 2017, 2, 5861−5872

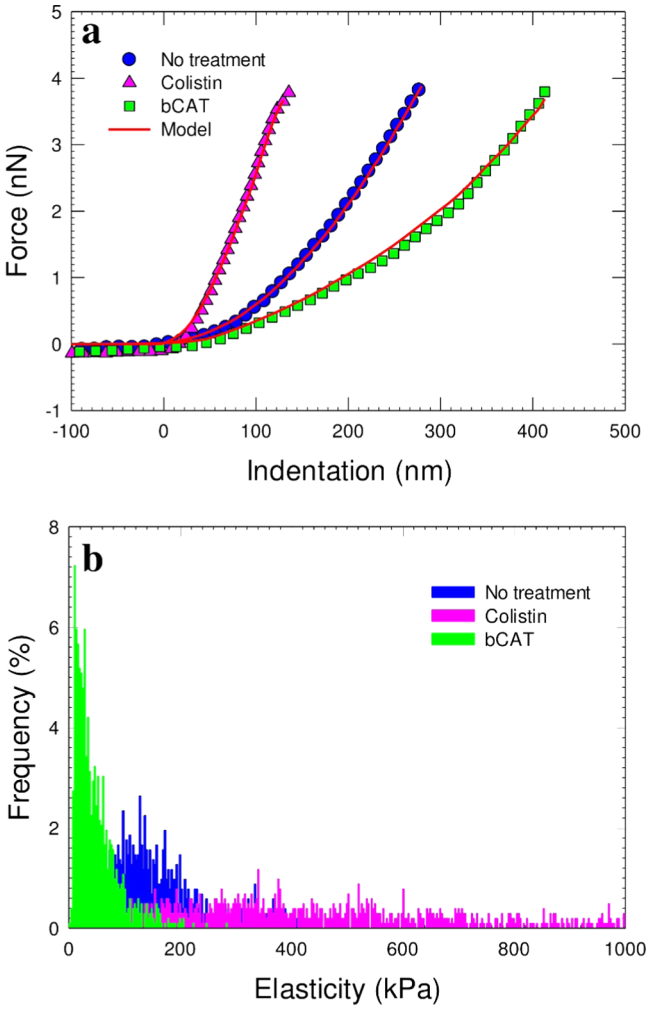


**Figure 6.** (a) Representative force−indentation curves (scatters) of *E. coli* biofilm with theoretical model (red line) before and after the action of AMPs. (b) Statistical distribution of the Young modulus values of *E. coli* biofilm before and after the action of AMPs.

**2.4. *E. coli* Biofilm Treated with Catestatin.** The MIC of catestatin for planktonic *E. coli* was measured at 60 $\mu$M. This value was in the range of those previously reported.[26] Figure 4b shows the spectral evolution of the 5.5 h old biofilm recorded during 24 h of exposure to catestatin at its MIC. The spectra were first dominated by the amide bands at around 1640 and 1540 $cm^{-1}$. This spectral signature was composed of amide bands already observed in the spectra of the reference biofilm. Additional amide bands appeared progressively at 1624 and 1531 $cm^{-1}$. The amide bands appeared 2 h after the injection of catestatin, and they increased throughout the course of the 24 h experiment. These bands were assigned to catestatin that accumulated on the bacteria, and the corresponding wavenumbers suggested a $\beta$-sheet conformation of the peptide.[50−52] Amide I bands of only equal intensities were observed at 1657 and 1623 $cm^{-1}$ for catestatin in water (Figure 4b). The occurrence of $\beta$-sheet was already detected in water and in a more hydrophobic solvent in other studies.[53,54] Thus, catestatin was likely to increase the $\beta$-sheet conformation probably by accumulation of catestatin in the vicinity of the bacterial membrane. Such a phenomenon has been reported by Jean-Francois et al. on a similar peptide, cateslytin, in the presence of negatively charged bacterial mimetic membranes.[55] The spectral profile in the region 1300−900 $cm^{-1}$ changed with respect to the reference biofilm. No typical bands of glycogen were observed, suggesting the inhibition of glycogen production by the peptide treatment. All of these changes indicated a dramatic change in bacterial metabolism. The BPSS procedure resolved two pure component spectra, which explained 96% of the total spectral variation of the spectra set (Figure 5b). SP1cat had the general spectral features of bacteria. However, the band shape of the region 1300−950 $cm^{-1}$ was deteriorated, suggesting a random structure for the nucleic acids (probably RNA[39]). SP2cat had the general spectral features of proteins.[39,40] The Amide I band showed an enhanced band at 1621 $cm^{-1}$ that was assigned to a $\beta$-sheet conformation. This band was already present in the spectrum of catestatin in water (see inset of Figure 5c), but the estimated quantity of the $\beta$-sheet conformation increased from about 45 to about 60% (from a decomposition procedure with Gaussian bands and taking into account possible errors coming from a nonperfect compensation of the water background). Figure 5d shows the relative concentration profiles calculated by the BPSS analysis. The estimated relative concentration C1cat of SP1cat increased until 7 h and then decreased slightly to reach a pseudoplateau. Bacteria multiplied on the surface during 6 h, and the successive decrease of C1cat suggested a partial loss of biomass after 7 h of the catestatin treatment. The estimated concentration C2cat of SP2cat increased very quickly during 3 h, and then this concentration was more or less stable for the rest of the experiment. The accumulation of catestatin reached its maximal value, leading to the end of metabolic activity and to a partial loss of biomass by detachment.

Figure 2i,j showed the epifluorescence images of the biofilm after 24 h of catestatin treatment. The GFP fluorescence was very weak (Figure 2i), suggesting an alteration of the bacterial metabolism. The bacteria stained with the *Bac*Light kit were homogeneously orange/red throughout the surface, reflecting damaged membranes (Figure 2j). The bacterial morphology was not impacted by the catestatin treatment. The rodlike bacterial shape was maintained, and it was in accordance with AFM images (Figure 3g−h). The average length was 2.2 ± 0.3 $\mu$m for a width of 0.8 ± 0.1 $\mu$m (Table 3). The cross sections (Figure 3i) indicated bacterial thickness of about 400 nm on an average. This value remained similar to the value measured for the nontreated biofilm. Holes were observed in the bacterial membranes (arrows on Figure 3h). Therefore, it can be suggested that the mechanism of catestatin action passes through a barrel stave or a toroidal pore mechanism.[18] The maximal indention depth measured at an applied force of 4 nN on the representative force curves was about 420 nm for the catestatin-treated biofilm. This value was 1.5 times greater than the one measured on the nontreated biofilm, reflecting softening of the bacterial membranes. Figure 6b shows a Gaussian distribution of the elastic modulus, with an average value of 48 ± 27 kPa, which was about 3 times lower with respect to the nontreated biofilm. The decrease in bacterial stiffness caused by AMPs derived from magainin was previously described by da Silva et al.[56]

**2.5. Is the Antimicrobial Peptide Action Irreversible against Sessile Bacteria?** After the AMP treatments, the biofilms were subjected to a fresh sterile nutritive medium to assess the efficiency of the treatment. The ATR-FTIR spectral evolutions are shown in Figure 4c,d. Concerning the biofilm treated with colistin, the spectra showed during 3 h (i) the rapid increase of bands at 1240, 1219, 1122, and 1085 $cm^{-1}$



DOI: 10.1021/acsomega.7b00644
*ACS Omega* 2017, 2, 5861−5872

assigned to nucleic acids, and (ii) a slight decrease of bands at 1646 and 1548 $cm^{-1}$ assigned to Amide I and II of proteins. This result suggested the high metabolic activity of intact cells and the partial loss of biomass from the highly damaged bacteria, respectively. After 3 h, all of the bands in the fingerprint region progressively increased again. The whole bands were assigned to the bacterial fingerprint, and this result suggested the bacterial repopulation (Figure 4c). The intact bacteria had recovered from the antimicrobial treatment. The epifluorescence images showed a very high coverage of the Ge surface by bacteria (almost 100%, Figure 2g,h), and multilayers of bacteria were observed. The bacteria had also recovered their original size and shape with an average length of 1.9 ± 0.3 $\mu$m. On the contrary, for the biofilm treated with catestatin, a strong decrease of the whole infrared signature was observed (Figure 4d). These spectral fingerprints, typical of bacteria, suggested a strong loss of the biomass from the surface of the Ge crystal. The bacteria therefore could not survive the peptide treatment and detached from the surface, and the peptide had an irreversible effect on the sessile bacteria. The epifluorescence pictures were in good agreement with the infrared results. They showed very few bacteria on the Ge surface after 17 h of flow of LB/10 (Figure 2k,l). Dark spots with undefined shapes after *Bac*Light staining were also present and corresponded probably to cell fragments.[36] The time evolution of the biofilm after the peptide treatments at the different MICs clearly highlighted two different modes of action. Whereas some bacteria were able to regrow and recolonize the crystal after the colistin treatment, this was not the case for the catestatin treatment. Emphasizing that both peptides have the same positive charge, the difference of activity should come from their secondary structure. First, the cyclic peptide with an acyl chain (colistin) was more destructive in terms of cell integrity with respect to the linear peptide (catestatin), in accordance with the literature.[21,57] Second, the MIC of catestatin was about 70 times higher than that of colistin but the bacterial growth was stopped irreversibly. At the MIC, the number of colistin molecules per bacteria was lower than that for catestatin, and therefore it can be explained that the bacterial growth kept going on in the presence of colistin. All of these elements underlined that excluding the possible intrinsic resistance of the bacteria, treatments with higher concentrations of colistin are necessary to determine the concentration required to stop irreversibly the biofilm growth to reach the catestatin performance.

## 3. CONCLUSIONS

In the present study, we combined several physical chemistry techniques to probe and monitor biochemical changes within a young *E. coli* biofilm subjected to a cyclic or a linear AMP. The combined techniques provided us new insights on the very different behaviors of the two AMPs. Colistin dramatically and harshly altered bacterial morphology and cell wall stiffness even though its action was not homogeneous on the bacterial population. Indeed, some bacteria remained intact after the treatment and bacterial repopulation was observed. Here, the cyclic AMP was found to have an impact on the nucleic acid production of the bacteria and to stiffen the bacterial cell wall. Besides, a subpopulation of bacteria is able to regrow after the cyclic AMP treatment. Conversely, no drastic changes in the bacterial morphology appeared under the catestatin treatment unless there was occurrence of nanopores in the bacterial membranes. However, the catestatin action was homogeneous and irreversible over the whole bacterial population. Indeed, all membranes were permeabilized, and the bacterial cell wall stiffness was reduced in such an irreversible way that those bacteria were washed out and unable to regrow after the treatment. It can be highlighted that this difference and the gain in antimicrobial activity may be related to the conformational flexibility of catestatin.

## 4. MATERIALS AND METHODS

**4.1. Chemicals and Synthetic Peptides.** Colistin sulfate salt, ampicillin, kanamycin, and phosphate saline buffer (PBS) were purchased from Sigma-Aldrich, France. Bovine catestatin has an amino acid sequence of RSMRLSFRAR-GYGFRGPGLQL, and it was purchased from ProteoGenix (Schiltigheim, France). The peptides were stored at −20 °C as a stock solution at 1 g/L in nonpyrogenic sterile water (Aqua B-Braun, Melsungen, Germany). Structures and physicochemical properties of colistin and catestin are reported in Table 1.

**4.2. Bacterial Strain and Culture Conditions.** The bacterial model used in this study is a Gram-negative *Escherichia coli* mutant called E2146, which is kindly provided by Institut Pasteur from Paris. This strain was constructed from *Escherichia coli* MG1655; it contains genes that make it fluorescent (green fluorescent protein, GFP) and is non-flagellated. It is also resistant to specific antibiotics. Strain E2146 constitutively produces the external ultrastructure type 1 *fimbriae*.[46] The bacterial stock was maintained at −80 °C. Bacteria were cultured in Lysogeny Broth (LB, Miller, Fluka) at 25 g/L in deionized water (Purelab Option, ELGA). All of the cultures were grown in a water bath at 37 ± 1 °C and under continuous agitation at 160 rpm. After an overnight subculture (16 h, with antibiotics, i.e., ampicillin and kanamycin), bacteria were cultivated in 200 mL of LB medium (without antibiotics) in 500 mL conical flasks with an initial optical density at 600 nm ($OD_{600}$, measured with a cell density meter, Fisherbrand) of 0.050 ± 0.005.

**4.3. Minimum Inhibitory Concentration (MIC) Determination.** MIC was determined by broth microdilution. An overnight subculture of the bacterial strain described above was diluted to $OD_{600}$ = 0.001. The diluted culture (90 $\mu$L) was plated in 96-well plates in the presence of catestatin or colistin at different concentrations. After 24 h of incubation, the microorganism growth was assessed by $OD_{600}$ using a Multiskan EX microplate spectrophotometer (Thermo Fisher Scientific). The MIC, defined as the lowest concentration of drug able to inhibit 100% of the inoculum, was determined from a modified Gompertz function, as described in previous studies.[58] Experiments were performed at least three times.

**4.4. Biofilm Submitted to Antibacterial Treatments.** Cells in the end of the exponential growth phase ($OD_{600}$ between 0.5 and 0.6) were harvested by centrifugation (5000*g*, 10 min, and 4 °C), and the pellet was resuspended in 200 mL of diluted 1:10 sterile LB medium (at 2.5 g/L, hereafter called LB/10). This suspension is hereafter called SEc0. Biofilms were initiated in LB/10 in flow cells containing a germanium (Ge) crystal. Conditions were adapted from the method described previously,[36,59] no preliminary conditioning film was established. SEc0 was pumped into the flow cell at 50 mL/h during 2.5 h to promote the bacterial adhesion (30 min in static mode and 2 h in flowing mode). For all subsequent experiments the flow rate was also set at 50 mL/h. Then, the bacterial suspension was replaced by LB/10 flow during 3 h to initiate biofilm development. Two flow cells were used for biofilm elaboration. For the infrared study, an IR-ATR flow cell



DOI: 10.1021/acsomega.7b00644
*ACS Omega* 2017, 2, 5861−5872

(SPECAC, Kent, United Kingdom) enclosing a Ge crystal was used, as described elsewhere.[31,36] For the AFM study, biofilms were grown on a disk of Ge in a homemade flow cell.[31] Briefly, this flow cell consists of a poly(methyl methacrylate) base plate that was milled out to form a shallow flow chamber and had an inlet and exit for liquid. Using a gasket, a glass microscope plate was clamped on the top of the base to seal the flow cell.

**4.5. Peptide Action on the 5.5 h Old Biofilm of *E. coli*.** The 5.5 h old biofilms were exposed for 24 h to either LB/10 medium, as the control experiment, or to the AMP at MICs in sterile LB/10 medium. The pH of all solutions was 7.0 ± 0.1. The sterile LB/10 medium solution (40 mL), with or without AMP, was injected in the flow cell into a new closed circuit in maintaining the same flow rate as in both previous steps. The inoculations of the LB/10 medium and the peptide solutions were carefully performed under sterile conditions, avoiding formation of air bubbles in the flow cell. An abiotic experiment was conducted with the same conditions, that is, sterile LB/10 medium was injected in the flow cell during 5.5 h in the open circuit, followed by the flow of the peptide solution during 24 h in the closed circuit. In another experiment, after the AMP treatment, the sessile bacteria were subjected to a new, 17 h long treatment in an open circulation of fresh LB/10 nutrient to assess whether the AMP treatment was irreversible or not. Two independently conducted measurements were performed for every experiment, and the results were consistent.

**4.6. ATR-FTIR Spectroscopy.** The ATR-FTIR spectra were recorded between 4000 and 800 $cm^{-1}$ on a Bruker Tensor 27 spectrometer equipped with a KBr beam splitter and a deuterated triglycine sulfate thermal detector. Spectra recording and data processing were performed using the Bruker OPUS 7.5 software. The resolution of the single beam spectra was 4 $cm^{-1}$. One hundred scans were collected per spectrum, corresponding to a 1 min accumulation time. All interferograms were Fourier-processed using the Mertz phase correction and a Blackman−Harris three-term apodization function. No ATR correction was performed. ATR-FTIR spectra are shown with an absorbance scale corresponding to $\log(R_{reference}/R_{sample})$, where $R$ is the internal reflectance of the device. A reference spectrum acquired immediately before the step under study was recorded. Hence, as an example, the spectra reflected only the time evolution of the cells' fingerprint in the 5.5 h old biofilm subjected to LB/10 with or without AMP. Water vapor subtraction was performed. All spectra were baseline corrected at 3580, 2750, 1800, and 900 $cm^{-1}$. FTIR measurements were performed at 21 ± 1 °C in an air-conditioned room. For the biofilm monitoring, an ATR-FTIR flow cell (SPECAC) enclosing a trapezoidal Ge crystal, with an incidence angle of 45°, yielded six internal reflections on the upper face in contact with the sample. In the course of biofilm monitoring experiments, ATR-FTIR spectra were recorded every 15 min. The penetration depth of the evanescent wave was about 0.42 and 0.59 $\mu$m at 1550 and 1100 $cm^{-1}$, respectively.[31] Thus, assuming a close contact of the bacteria with the ATR crystal, a single layer of bacteria was analyzed.

**4.7. Curve Resolution Analysis: Bayesian Positive Source Separation.** The resolution of pure component spectra from the "mixture" spectra without any a priori information was performed with a statistical method of spectral mixture analysis called BPSS for Bayesian positive source separation. It was developed on the basis of the Bayesian estimation theory and Markov Chain Monte Carlo methods. Briefly, in the mixture analysis method, the spectral data sets resulting from observations of multicomponent substances are interpreted as a weighted sum of the unknown pure component spectra. The mixing model assumes that $m$ measured data are linear combinations of $p$ unknown pure component spectra. Each mixing coefficient is proportional to the concentration of the $j$th pure component in the $i$th mixture. Additive noise terms represent measurement errors and model imperfections. By assuming a known number of components, the mixture analysis aim is to estimate the pure component spectra and the mixing coefficient profiles from the mixture spectra.[60,61] It is possible to obtain relative concentrations by using BPSS and a mass-balance constraint without any calibration reference, which allows avoiding any personal subjective estimation. It must be emphasized that these concentrations are relative concentrations because they are weighted by the intensity of the normalized pure component spectra and not by a separate calibration. The data processing was applied to 95 ATR-FTIR spectra recorded during the flow of LB/10 with or without peptide in the closed circuit from 1 to 24 h of the flow. The analyses were performed on the spectral fingerprint region 1800−900 $cm^{-1}$.

**4.8. Atomic Force Microscopy.** AFM images and force spectroscopy measurements were performed using an MFP3D-BIO instrument (Asylum Research Technology, Atomic Force F&E GmbH, Manheim, Germany). The *E. coli* biofilm grown onto the Ge surface was gently rinsed with a PBS buffer solution and slightly dried with nitrogen (0.2 bar for 2 min) before the morphology analysis by AFM. Topographical images of the biofilms were performed by contact mode AFM. Silicon nitride cantilevers of conical shape purchased from Atomic Force (OMCL-TR400PSA-3, Olympus, Japan), with spring constant of about 20−25 pN/nm used for both imaging and nanomechanical measurements. All images were recorded with a resolution of 512 × 512 pixels and a scan rate of 1 Hz. Nanomechanical properties of the biofilms were measured in PBS buffer solution (pH 7.4) by recording at least three force−volume Images (FVIs) at different locations over the biofilm, each consisting of a grid of 32-by-32 force curves performed with an approach rate of 2 $\mu$m/s. The bacterial Young modulus $E$ was calculated by analyzing the force−indentation curves according to the Sneddon model.[62,63] In this model, the Young modulus is related to the applied force according to the equation given below

$$F = \frac{2E\tan(\alpha)}{\pi(1-\nu^2)} R^{1/2}\delta^2 \cdot f_{BECC} \quad (1)$$

where $\delta$ is the indentation depth, $\nu$ is the Poisson coefficient, $\alpha$ is the semitop angle of the tip, and $f_{BECC}$ is the bottom effect cone correction function that takes into account the presence of the substrate stiffness. All of the FVI were analyzed by an automatic Matlab algorithm described elsewhere,[64] and the average values given in this work were calculated from at least 3072 force curves.

**4.9. Fluorescence Optical Microscopy.** The biofilms at the end of the experiments were analyzed by fluorescence microscopy using intrinsic fluorescence of GFP and the *Bac*Light stain kit (L7012; Molecular Probes, Eugene) to determine the permeability of the sessile cells and the average bacterial surface coverage in the absence and presence of the AMP, as described elsewhere.[36] With this kit, bacteria with intact membranes exhibit green fluorescence, whereas bacteria with damaged membranes show red fluorescence. We have



DOI: 10.1021/acsomega.7b00644
ACS Omega 2017, 2, 5861−5872

beforehand verified on planktonic bacteria that the *Bac*Light stain kit is compatible with GFP fluorescent bacteria. The ATR cell was demounted; the Ge crystal was carefully removed, and rinsed with nonpyrogenic sterile water to remove nonadherent cells. The *Bac*Light solution was laid on the crystal and stained for 20 min in the dark at 21 ± 1 °C. The crystal was then rinsed with nonpyrogenic sterile water to eliminate excess *Bac*Light solution and wicked dry with a filter paper to remove excess water. The sample was mounted in *Bac*Light mounting oil, as described by the instructions provided by the manufacturer. Both fluorescence images were acquired simultaneously with the 100× oil immersion objective of an Olympus BX51 microscope equipped with an Olympus XC50 camera. Buffered glycerin (40% PBS + 60% glycerol, v/v) was used for the mounting of the sample in the case of the observation of GFP fluorescence.

## AUTHOR INFORMATION


### Corresponding Authors

*E-mail: fabienne.quiles@univ-lorraine.fr (F.Q.).
*E-mail: gregory.francius@univ-lorraine.fr (G.F.).

### ORCID

Grégory Francius: 0000-0001-8533-9449


### Notes

The authors declare no competing financial interest.

## ACKNOWLEDGMENTS

The authors are indebted to the financial support of Ministère de l'Enseignement Supérieur et de la Recherche (MESR), Institut Jean Barriol (IJB), Région Grand Est and Université de Lorraine. We greatly acknowledge Dr. Céline Marban and Dr. Marie-Hélène Metz-Boutigues for the MIC measurements. We also thank Dr. Christophe Beloin and Prof. Jean-Marc Ghigo from Institut Pasteur Paris for the supplying of *E. coli* and Dr. Grégoire Herzog for the proofreading and correction of this manuscript.

## REFERENCES


(1) Cassir, N.; Rolain, J.-M.; Brouqui, P. A new strategy to fight antimicrobial resistance: the revival of old antibiotics. *Front. Microbiol.* **2014**, *5*, No. 551.
(2) Orsi, G. B.; Falcone, M.; Venditti, M. Surveillance and management of multidrug-resistant microorganisms. *Expert Rev. Anti-Infect. Ther.* **2011**, *9*, 653−679.
(3) Giamarellou, H. Treatment options for multidrug-resistant bacteria. *Expert Rev. Anti-Infect. Ther.* **2006**, *4*, 601−618.
(4) Williams, K. J.; Bax, R. P. Challenges in developing new antibacterial drugs. *Curr. Opin. Invest. Drugs* **2009**, *10*, 157−163.
(5) Costerton, J. W. Introduction to biofilm. *Int. J. Antimicrob. Agents* **1999**, *11*, 217−221.
(6) Patel, R. Biofilms and antimicrobial resistance. *Clin. Orthop. Relat. Res.* **2005**, 41−47.
(7) Bridier, A.; Briandet, R.; Thomas, V.; Dubois-Brissonnet, F. Resistance of bacterial biofilms to disinfectants: a review. *Biofouling* **2011**, *27*, 1017−1032.
(8) Høiby, N.; Bjarnsholt, T.; Givskov, M.; Molin, S.; Ciofu, O. Antibiotic resistance of bacterial biofilms. *Int. J. Antimicrob. Agents* **2010**, *35*, 322−332.
(9) Mojsoska, B.; Jenssen, H. Peptides and Peptidomimetics for Antimicrobial Drug Design. *Pharmaceuticals* **2015**, *8*, 366−415.
(10) Hancock, R. E. W.; Sahl, H. G. Antimicrobial and host-defense peptides as new anti-infective therapeutic strategies. *Nat. Biotechnol.* **2006**, *24*, 1551−1557.
(11) Shai, Y. Mode of action of membrane active antimicrobial peptides. *Biopolymers* **2002**, *66*, 236−248.
(12) Guilhelmelli, F.; Vilela, N.; Albuquerque, P.; Derengowski, L. d. S.; Silva-Pereira, I.; Kyaw, C. M. Antibiotic development challenges: the various mechanisms of action of antimicrobial peptides and of bacterial resistance. *Front. Microbiol.* **2013**, *4*, No. 353.
(13) Epand, R. M.; Vogel, H. J. Diversity of antimicrobial peptides and their mechanisms of action. *Biochim. Biophys. Acta, Biomembr.* **1999**, *1462*, 11−28.
(14) Nguyen, L. T.; Haney, E. F.; Vogel, H. J. The expanding scope of antimicrobial peptide structures and their modes of action. *Trends Biotechnol.* **2011**, *29*, 464−472.
(15) Lee, T. H.; Hall, K. N.; Aguilar, M. I. Antimicrobial Peptide Structure and Mechanism of Action: A Focus on the Role of Membrane Structure. *Curr. Top. Med. Chem.* **2016**, *16*, 25−39.
(16) Wimley, W. C. Describing the Mechanism of Antimicrobial Peptide Action with the Interfacial Activity Model. *ACS Chem. Biol.* **2010**, *5*, 905−917.
(17) Nicolas, P. Multifunctional host defense peptides: intracellular-targeting antimicrobial peptides. *FEBS J.* **2009**, *276*, 6483−6496.
(18) Brogden, K. A. Antimicrobial peptides: Pore formers or metabolic inhibitors in bacteria? *Nat. Rev. Microbiol.* **2005**, *3*, 238−250.
(19) Hwang, P. M.; Vogel, H. J. Structure-function relationships of antimicrobial peptides. *Biochem. Cell Biol.* **1998**, *76*, 235−246.
(20) Ganz, T. Defensins: Antimicrobial peptides of innate immunity. *Nat. Rev. Immunol.* **2003**, *3*, 710−720.
(21) Davies, J. S. The cyclization of peptides and depsipeptides. *J. Pept. Sci.* **2003**, *9*, 471−501.
(22) Hancock, R. E. W.; Falla, T. J. Antimicrobial peptides: broad-spectrum antibiotics from nature. *Clin. Microbiol. Infect.* **1996**, *1*, 226−229.
(23) Abdelbaqi, S.; Deslouches, B.; Steckbeck, J.; Montelaro, R.; Reed, D. S. Novel engineered cationic antimicrobial peptides display broad-spectrum activity against *Francisella tularensis*, *Yersinia pestis* and *Burkholderia pseudomallei*. *J. Med. Microbiol.* **2016**, *65*, 188−194.
(24) Briolat, J.; Wu, S. D.; Mahata, S. K.; Gonthier, B.; Bagnard, D.; Chasserot-Golaz, S.; Helle, K. B.; Aunis, D.; Metz-Boutigue, M. H. New antimicrobial activity for the catecholamine release-inhibitory peptide from chromogranin A. *Cell. Mol. Life Sci.* **2005**, *62*, 377−385.
(25) Mahata, S. K.; Mahata, M.; Fung, M. M.; O'Connor, D. T. Catestatin: A multifunctional peptide from chromogranin A. *Regul. Pept.* **2010**, *162*, 33−43.
(26) Radek, K. A.; Lopez-Garcia, B.; Hupe, M.; Niesman, I. R.; Elias, P. M.; Taupenot, L.; Mahata, S. K.; O'Connor, D. T.; Gallo, R. L. The neuroendocrine peptide catestatin is a cutaneous antimicrobial and induced in the skin after injury. *J. Invest. Dermatol.* **2008**, *128*, 1525−1534.
(27) Özçelik, H.; Vrana, N. E.; Gudima, A.; Riabov, V.; Gratchev, A.; Haikel, Y.; Metz-Boutigue, M. H.; Carrado, A.; Faerber, J.; Roland, T.; Kluter, H.; Kzhyshkowska, J.; Schaaf, P.; Lavalle, P. Harnessing the Multifunctionality in Nature: A Bioactive Agent Release System with Self-Antimicrobial and Immunomodulatory Properties. *Adv. Healthc. Mater.* **2015**, *4*, 2026−2036.
(28) Falagas, M. E.; Kasiakou, S. K. Colistin: The revival of polymyxins for the management of multidrug-resistant gram-negative bacterial infections. *Clin. Infect. Dis.* **2005**, *40*, 1333−1341.
(29) Li, J.; Nation, R. L.; Turnidge, J. D.; Milne, R. W.; Coulthard, K.; Rayner, C. R.; Paterson, D. L. Colistin: the re-emerging antibiotic for multidrug-resistant Gram-negative bacterial infections. *Lancet Infect. Dis.* **2006**, *6*, 589−601.
(30) Spapen, H.; Jacobs, R.; Van Gorp, V.; Troubleyn, J.; Honore, P. M. Renal and neurological side effects of colistin in critically ill patients. *Ann. Intensive Care* **2011**, *1*, No. 14.
(31) Quilès, F.; Humbert, F.; Delille, A. Analysis of changes in attenuated total reflection FTIR fingerprints of *Pseudomonas fluorescens* from planktonic state to nascent biofilm state. *Spectrochim. Acta, Part A* **2010**, *75*, 610−616.




DOI: 10.1021/acsomega.7b00644
*ACS Omega* 2017, 2, 5861−5872

(32) Filip, Z.; Hermann, S. An attempt to differentiate Pseudomonas spp. and other soil bacteria by FT-IR spectroscopy. *Eur. J. Soil Biol.* **2001**, *37*, 137−143.
(33) Maquelin, K.; Kirschner, C.; Choo-Smith, L. P.; van den Braak, N.; Endtz, H. P.; Naumann, D.; Puppels, G. J. Identification of medically relevant microorganisms by vibrational spectroscopy. *J. Microbiol. Methods* **2002**, *51*, 255−271.
(34) Legal, J. M.; Manfait, M.; Theophanides, T. Applications of FTIR spectroscopy in structural studies of cells and bacteria. *J. Mol. Struct.* **1991**, *242*, 397−407.
(35) Naumann, D. Some ultrastructural information on intact, living bacterial cells and related cell-wall fragments as given by FTIR. *Infrared Phys.* **1984**, *24*, 233−238.
(36) Quilès, F.; Saadi, S.; Francius, G.; Bacharouche, J.; Humbert, F. In situ and real time investigation of the evolution of a *Pseudomonas fluorescens* nascent biofilm in the presence of an antimicrobial peptide. *Biochim. Biophys. Acta, Biomembr.* **2016**, *1858*, 75−84.
(37) Quilès, F.; Humbert, F. On the production of glycogen by *Pseudomonas fluorescens* during biofilm development: an in situ study by attenuated total reflection-infrared with chemometrics. *Biofouling* **2014**, *30*, 709−718.
(38) Wilson, W. A.; Roach, P. J.; Montero, M.; Baroja-Fernandez, E.; Munoz, F. J.; Eydallin, G.; Viale, A. M.; Pozueta-Romero, J. Regulation of glycogen metabolism in yeast and bacteria. *FEMS Microbiol. Rev.* **2010**, *34*, 952−985.
(39) Naumann, D. FT-infrared and FT-Raman spectroscopy in biomedical research. *Appl. Spectrosc. Rev.* **2001**, *36*, 239−298.
(40) Suci, P. A.; Vrany, J. D.; Mittelman, M. W. Investigation of interactions between antimicrobial agents and bacterial biofilms using attenuated total reflection Fourier transform infrared spectroscopy. *Biomaterials* **1998**, *19*, 327−339.
(41) Young, K. D. Bacterial morphology: why have different shapes? *Curr. Opin. Microbiol.* **2007**, *10*, 596−600.
(42) Wallace, S. J.; Li, J.; Nation, R. L.; Prankerd, R. J.; Velkov, T.; Boyd, B. J. Self-Assembly Behavior of Colistin and Its Prodrug Colistin Methanesulfonate: Implications for Solution Stability and Solubilization. *J. Phys. Chem. B* **2010**, *114*, 4836−4840.
(43) Soon, R. L.; Nation, R. L.; Hartley, P. G.; Larson, I.; Li, J. Atomic Force Microscopy Investigation of the Morphology and Topography of Colistin-Heteroresistant *Acinetobacter baumannii* Strains as a Function of Growth Phase and in Response to Colistin Treatment. *Antimicrob. Agents Chemother.* **2009**, *53*, 4979−4986.
(44) Cochran, W. L.; McFeters, G. A.; Stewart, P. S. Reduced susceptibility of thin *Pseudomonas aeruginosa* biofilms to hydrogen peroxide and monochloramine. *J. Appl. Bacteriol.* **2000**, *88*, 22−30.
(45) Das, J. R.; Bhakoo, M.; Jones, M. V.; Gilbert, P. Changes in the biocide susceptibility of *Staphylococcus epidermidis* and *Escherichia coli* cells associated with rapid attachment to plastic surfaces. *J. Appl. Bacteriol.* **1998**, *84*, 852−858.
(46) Francius, G.; Polyakov, P.; Merlin, J.; Abe, Y.; Ghigo, J. M.; Merlin, C.; Beloin, C.; Duval, J. F. L. Bacterial Surface Appendages Strongly Impact Nanomechanical and Electrokinetic Properties of *Escherichia coli* Cells Subjected to Osmotic Stress. *PLoS One* **2011**, *6*, No. e20066.
(47) Formosa, C.; Herold, M.; Vidaillac, C.; Duval, R. E.; Dague, E. Unravelling of a mechanism of resistance to colistin in *Klebsiella pneumoniae* using atomic force microscopy. *J. Antimicrob. Chemother.* **2015**, *70*, 2261−2270.
(48) Soon, R. L.; Nation, R. L.; Harper, M.; Adler, B.; Boyce, J. D.; Tan, C. H.; Li, J.; Larson, I. Effect of colistin exposure and growth phase on the surface properties of live *Acinetobacter baumannii* cells examined by atomic force microscopy. *Int. J. Antimicrob. Agents* **2011**, *38*, 493−501.
(49) Mortensen, N. P.; Fowlkes, J. D.; Sullivan, C. J.; Allison, D. P.; Larsen, N. B.; Molin, S.; Doktycz, M. J. Effects of Colistin on Surface Ultrastructure and Nanomechanics of *Pseudomonas aeruginosa* Cells. *Langmuir* **2009**, *25*, 3728−3733.
(50) Kong, J.; Yu, S. Fourier transform infrared spectroscopic analysis of protein secondary structures. *Acta Biochim. Biophys. Sin.* **2007**, *39*, 549−559.
(51) Goormaghtigh, E.; Ruysschaert, J. M.; Raussens, V. Evaluation of the information content in infrared spectra for protein secondary structure determination. *Biophys. J.* **2006**, *90*, 2946−2957.
(52) Nagant, C.; Pitts, B.; Nazmi, K.; Vandenbranden, M.; Bolscher, J. G.; Stewart, P. S.; Dehaye, J. P. Identification of Peptides Derived from the Human Antimicrobial Peptide LL-37 Active against Biofilms Formed by *Pseudomonas aeruginosa* Using a Library of Truncated Fragments. *Antimicrob. Agents Chemother.* **2012**, *56*, 5698−5708.
(53) Tsigelny, I.; Mahata, S. K.; Taupenot, L.; Preece, N. E.; Mahata, M.; Khan, I.; Parmer, R. J.; O'Connor, D. T. Mechanism of action of chromogranin A on catecholamine release: molecular modeling of the catestatin region reveals a $\beta$-strand/loop/$\beta$-strand structure secured by hydrophobic interactions and predictive of activity. *Regul. Pept.* **1998**, *77*, 43−53.
(54) Jean-François, F.; Khemtemourian, L.; Odaert, B.; Castano, S.; Grelard, A.; Manigand, C.; Bathany, K.; Metz-Boutigue, M. H.; Dufourc, E. J. Variability in secondary structure of the antimicrobial peptide Cateslytin in powder, solution, DPC micelles and at the air-water interface. *Eur. Biophys. J.* **2007**, *36*, 1019−1027.
(55) Jean-François, F.; Castano, S.; Desbat, B.; Odaert, B.; Roux, M.; Metz-Boutigue, M. H.; Dufourc, E. J. Aggregation of cateslytin beta-sheets on negatively charged lipids promotes rigid membrane domains. A new mode of action for antimicrobial peptides? *Biochemistry* **2008**, *47*, 6394−6402.
(56) da Silva, A., Jr.; Teschke, O. Effects of the antimicrobial peptide PGLa on live *Escherichia coli*. *Biochim. Biophys. Acta, Mol. Cell Res.* **2003**, *1643*, 95−103.
(57) Mika, J. T.; Moiset, G.; Cirac, A. D.; Feliu, L.; Bardaji, E.; Planas, M.; Sengupta, D.; Marrink, S. J.; Poolman, B. Structural basis for the enhanced activity of cyclic antimicrobial peptides: The case of BPC194. *Biochim. Biophys. Acta, Biomembr.* **2011**, *1808*, 2197−2205.
(58) Lambert, R. J. W.; Pearson, J. Susceptibility testing: accurate and reproducible minimum inhibitory concentration (MIC) and non-inhibitory concentration (NIC) values. *J. Appl. Bacteriol.* **2000**, *88*, 784−790.
(59) Fahs, A.; Quilès, F.; Jamal, D.; Humbert, F.; Francius, G. In Situ Analysis of Bacterial Extracellular Polymeric Substances from a *Pseudomonas fluorescens* Biofilm by Combined Vibrational and Single Molecule Force Spectroscopies. *J. Phys. Chem. B* **2014**, *118*, 6702−6713.
(60) Dobigeon, N.; Moussaoui, S.; Tourneret, J. Y.; Carteret, C. Bayesian separation of spectral sources under non-negativity and full additivity constraints. *Signal Process.* **2009**, *89*, 2657−2669.
(61) Moussaoui, S.; Carteret, C.; Brie, D.; Mohammad-Djafari, A. Bayesian analysis of spectral mixture data using Markov chain Monte Carlo methods. *Chemom. Intell. Lab. Syst.* **2006**, *81*, 137−148.
(62) Sneddon, I. N. The relation between load and penetration in the axisymmetric Boussinesq problem for a punch of arbitrary profile. *Int. J. Eng. Sci.* **1965**, *3*, 47−57.
(63) Gavara, N.; Chadwick, R. S. Determination of the elastic moduli of thin samples and adherent cells using conical AFM tips. *Nat. Nanotechnol.* **2012**, *7*, 733−736.
(64) Polyakov, P.; Soussen, C.; Duan, J. B.; Duval, J. F. L.; Brie, D.; Francius, G. Automated Force Volume Image Processing for Biological Samples. *PLoS One* **2011**, *6*, No. e18887.



DOI: 10.1021/acsomega.7b00644
*ACS Omega* 2017, 2, 5861−5872